On Nitrogen Pick-up during Pressure-ESR of Austenitic Steels

A.D. Patel [1],J. Reitz [2], J. H. Magee [1], R. Smith [1], G. Maurer [1], B. Friedrich [2]

1. Carpenter Technology, Corp, 101 W Bern St
Reading PA 19610, USA
2. IME Process Metallurgy and Metal Recycling
RWTH Aachen University, D-52056, Aachen, Germany

(Pressure ESR, high nitrogen steels)

Abstract

In the 1970's, the 200 series stainless steels were pressure melted to attain a higher nitrogen content. It has been reported that these alloys had higher strength and superior corrosion resistance. In austenitic steels, nitrogen solubility closely follows Sieverts law, and actually increases at lower temperature. Over the years, different pressure melting techniques have been proposed to increase the dissolution of nitrogen. Pressure Electro Slag Remelting (PESR) has emerged as the most robust process for producing high nitrogen steels of the desired qualities. The nitrogen is introduced into the melt by dissolving nitrogen bearing additives during the remelting process, in order to overcome slow mass transfer at the gas-melt interface inherent in competing processes. In this study, a laboratory scale PESR furnace was used to examine the effect of furnace pressure and addition of different compounds to the slag on nitrogen distribution in a Fe-Cr-Mn-N alloy system. Experimental parameters were obtained by modeling this alloy system using commercially available software. Small ingots of 160 mm (6 inch) diameter ingots were cast, sectioned, characterized and the composition was analyzed. The PESR processing parameters, along with nitrogen variation on the ingot's horizontal and vertical axis, are presented in this paper.

Introduction

The use of the 200 series stainless steels came about when nickel was scarce. This occurred during World War II, the Korean War, and again 20 years later after a drastic curtailment of the nickel supply in 1969. Scarcity of nickel is not the critical issue in the 21st century, but rather the volatility in the price of nickel. In 2006-07, the London Metal Exchange (LME) price of nickel went from $6 to $23. This has led metallurgists to consider alternative low nickel, high-nitrogen alloys, especially when their current stainless alloy contains 12-30%Ni. The benefits of nitrogen in steels include increased strength and chloride corrosion resistance and are well documented in proceedings of conferences dedicated to this subject /1/.

In conventional steel making, nitrogen is often introduced into the melt using either a master alloy, like ferro-chrome nitride, or in a process like Argon Oxygen Decarburization (AOD), where it can be blown into the melt. However, in these processes, the maximum amount of nitrogen that can be added to the alloy is limited by its solubility at the casting temperature under atmospheric pressure. Casting under higher pressures increases the solubility limit of nitrogen in steels. Over the years, researchers have proposed several processing routes such as pressure induction melting, arc ESR, and PESR to produce high nitrogen steels /2/. The latter of these has emerged as the most robust, safe and reliable process for making these alloys /3/. Since CaF2 based slags have virtually no solubility for nitrogen, it is actually introduced into the ingot through nitrogen bearing additives. The furnace pressure merely serves to increase the amount of nitrogen that can be dissolved into the alloy /4/.

Very high-nitrogen stainless steels, such as BioDur ® 108, have unique properties and problems associated with the addition of 1% nitrogen. Annealed yield strength is 2.5X higher than conventional 300 stainless steels due to the interstitial strengthening characteristics of nitrogen; yet toughness and ductility do not appreciably drop-off. The alloy's high strain hardening component results in ultimate tensile strengths greater than 300ksi (2070MPa) with no deformation-induced martensite when cold worked 65%. In addition, corrosion properties are improved. The pitting resistance equivalent number (PREN) has nitrogen 16X more effective than chromium with respect to its effect on pitting resistance. Finally, very high-nitrogen additions can result in an austenitic structure without the need for nickel. This has a significant cost benefit and can also be used for medical applications where nickel-free alloys are sought out when allergic reactions to nickel are a concern. There are, however, problems associated with very high-nitrogen additions. Higher forces are encountered when machining or hot and cold forming these alloys. Also, nitrogen can outgas when welding due to the criticality of nitrogen solubility in these alloys.

The purpose of this study was to examine the effect of melting parameters on nitrogen distribution in laboratory size PESR ingots, not on traditional ESR parameters like power input, slag type and volume. This is an ongoing research program between Carpenter R&D and the Industrial and Manufacturing Engineering (IME) department at Aachen University and is directed towards examining the effect of processing parameters such as furnace pressure and type of additives on the chemistry of alloy steels.

Pressure ESR Furnace

The PESR furnace located in the IME department, at Aachen University is capable of operating under inert-gas at a maximum pressure of 50 bar. It is equipped with a 5 kA power supply, and a new control system. The nominal electrode diameter is 110 mm, and the ingot diameter is 150 mm. The furnace is equipped with two bunkers and screw feeders for introducing additives during remelting as shown in Figure 1. The feeders are driven by pneumatic cylinders which turn the feeder screw by a wrench-like set-up in 90° steps. With every turn, a controlled amount of the additive is extracted from the respective bunker and charged to the melt. The number of wrenching impulses per minute can be set independently for every feeder in the furnace control system. The furnace interior, the bunkers, and the cooling water are all maintained at the operating pressure. This furnace is not equipped with load cells, and the melt rate is estimated from ram travel. For a smooth start-up, turnings are used with slag in the annular region between the electrode and crucible.

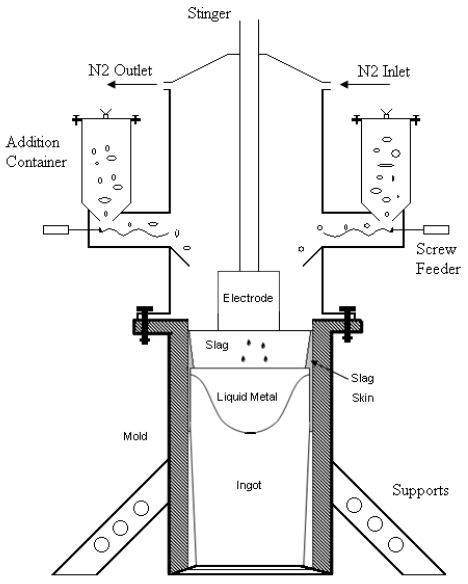

Figure 1: Sketch of the PESR furnace

A brief review of nitrogen solubility and interaction parameters

Detailed reviews of nitrogen solubility and production of high nitrogen steels are available in surveys such as that of Feichtinger and Stein and others /5, 6/. For a diatomic gas like nitrogen, the solubility reaction in liquid iron is generally written as:

$$\tfrac{1}{2} N_2 = [N] \qquad (1)$$

where brackets [ ] indicate the component is dissolved in liquid metal. The standard free energy of equation 1 can be used to calculate the equilibrium constant, K_{eq}, which can be used to relate the solubility (given in weight percent) to partial pressure:

$$K_{eq} = \frac{f_N \left[\%N\right]}{\left(p_{N_2}\right)^{1/2}} \tag{2}$$

where p_{N2} is the partial pressure of nitrogen in atm and f_N is the nitrogen activity coefficient. The following equation is used to calculate the activity coefficient for nitrogen, which includes 2nd order terms to account for high alloying element levels:

$$\log f_N = \Sigma e_N^j \left[\%j\right] + \Sigma r_N^j \left[\%j\right]^2 + \Sigma r_N^{j-k} \left[\%j\right]\left[\%k\right] \tag{3}$$

where e^j_N and r^j_N represent the 1st and 2nd order interaction parameters for the effect of component j on nitrogen, and $r^{j\text{-}k}_N$ is the 2nd order co-interaction parameter for the effect of component j and k on nitrogen. Interaction parameters are normally reported either as numerical values at 1600 C, or as temperature dependent terms.

In pure iron and low alloy steels, nitrogen is known to follow Sieverts' Law, in which solubility is directly proportional to the square root of partial pressure, however in stainless and related alloys, the solubility deviates from the law at elevated pressures. To account for the deviation, use of a self-interaction parameter for nitrogen has been cited /5/. Elements that increase solubility of nitrogen include chromium, manganese and molybdenum. Although elements such as titanium and vanadium can have a greater effect on solubility, they readily form nitrides and effectively establish their own limit. Nickel, silicon, and carbon decrease solubility.

Calculated nitrogen solubility for selected alloys

Estimations of nitrogen solubility were carried out on several different alloys using a set of interaction parameters as described above and also using ThermoCalc Classic (TCC) with the TCFE5 database. The equilibrium constant of equation 1 was calculated from the following /7/:

$$\log K_{eq} = -518/T - 1.063 \tag{4}$$

To calculate the activity coefficient, temperature dependent interaction parameters were used for Cr, Mn, Ni and Mo /8, 9/ and constant values for carbon, vanadium /10/ and the nitrogen self-interaction parameter /11/. Simplified versions of four different alloy compositions are given in Table 1 and resulting estimations of solubility are presented in Figure 2. TCC was used for two of the alloys as it predicted more accurate solubility for existing compositions produced at one atmospheric pressure. Results from TCC also indicated that deviations from Sieverts' Law were taken into account. These calculations also show that for these compositions, solubility increases with decreasing temperature.

Alloy Name	Cr	Mn	Ni	Mo	C	V
Biodur 108	21	23				
15-15HS	19	18	2			
22-13-5	21	5	13	1.8		0.2
2205	22	2	5	2.6		

Table 1. Assumed compositions for calculation of nitrogen solubility in Figure 2.

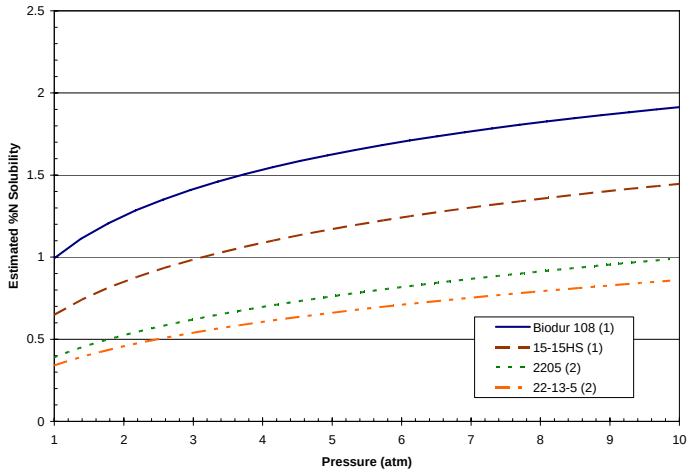

Figure 2. Nitrogen solubility versus pressure at 1600 C for various alloys. In the legend (1) denotes use of interaction parameters and (2) use of ThermoCalc with TCFE5.

Experimental Plan

The main purpose of these trials was to examine the effect of furnace pressure and nitrogen bearing additives on nitrogen solubility in a high chrome, high manganese austenitic steel, such as BioDur ® 108 during PESR. The electrodes were 100 mm in diameter and were cast using a laboratory scale Vacuum Induction Melting (VIM) furnace with a nitrogen content of 0.82 wt %. The goal was to increase it by 24% and 49% using Si_3N_4 and FeCrN as shown in Table 2. The furnace pressure set-point was selected to be higher than the theoretically calculated value. The feed rate (FR) of the additive was determined by using the following relationship,

$$FR = \frac{\Delta N}{N_{additive}} \dot{m} \qquad (1)$$

Where ΔN is the difference between the nitrogen content of the ingot and electrode, $N_{additive}$ is the percentage of nitrogen in the additive, and m is the melt rate set-point.

melt no	elec.dia. top (cm)	elec. dia. bottom (cm)	electrode weight (kg)	electrode N (wt%)	electrode Si (wt%)	electrode Cr (wt%)	Key PESR parameter	furnace pressure set-point (Bar)	target ingot N (wt%)	additive	melt rate set-point (kg/min)	feed rate set-point (gm/min)
5	10	11	72	0.82	0.15	21.19	low pressure, Si3N4	4	1.02	Si3N4	1.45	13
6	10	11	70	0.82	0.15	21.19	low pressure & FeCrN	4	1.02	FeCrN	1.45	46
7	10	11	72	0.82	0.15	21.19	high pressure, Si3N4	6	1.22	Si3N4	1.45	26

Table 2: Electrode and target ingot chemistry for these trials

Experimental Procedure

Each experiment consisted of feeder calibration and preparation prior to the melt, followed by the melt using a pre-programmed profile.

The Silicon nitride (grade B7) was in powder form of about 10 μm size. To allow for proper feeding through the bunkers and a consistent feed rate, the material was mixed in a 2:1 ratio with sand. The feed rate of the bunkers was calibrated before the trials at different feeding speeds. Calibration yields a linear relationship between impulses / minute of the pneumatic cylinders and g / minute of charged SiN & SiO_2 mixture. On the other hand, the FeCrN used was in the form of granules, 1-10 mm in diameter.

For start-up, nearly a kilogram of low carbon construction steel turnings was used. The turnings were placed in a bin located on the starter plate of the crucible and fastened with hooks. The crucible was then placed positioned over the starter plate, and the entire assembly was secured. The crucible was lowered into the furnace tank and the electrode that is attached to the ram is lowered into the crucible. Then, 3.75 kg of standard CaF2 60%/ CaO 20%/Al_2O_3 20% slag was

distributed around the turnings, in the annular region between the electrode and crucible. After this, the additives were charged with the total weight split between the two feeders and then they were sealed. Both feeders were primed for 60 seconds which has proven to be sufficient for complete filling of the screws for adequate feeding. The furnace head was then bolted, cooling water circuits were started, and the melting chamber was evacuated down to 1mbar with a vacuum pump and backfilled with nitrogen. The furnace was now ready for melting.

The process was started in electric arc mode under current control with a set-point of 4 kA at 28 V. After the slag was completely molten, current control was superseded by a constant power control at 110 kW with a quick ramp-up to 130 kW and slow ramp-down to 105kW after the start-up. With the switch to power control, electrode immersion/ram travel was subjected to resistance control at a set-point of 12 mOhm. After the 130 kW power-up, ram-travel was refined by "Swing control" at a set-point of 10% of the absolute slag resistance. Simultaneously with the switch to power control, feeding of the nitrogen additive was ramped up to the desired feed rate. At the end of the melt, a short hot-topping phase was initiated. The typical pressure variation during the melt is shown in Figure 3, and representative trace of the power and current variation is shown in Figure 4.

A short duration after the melt was completed, the furnace pressure was released and the furnace seal was broken. The furnace was unbolted, and the ingot was extracted from the crucible, and weighed. The slag cap was measured, weighed, manually broken and sealed in plastic bags to avoid moisture pickup. The feeders were emptied and leftover Si_3N_4 & sand mix was weighed. On the rim of the crucible, the amount of flue-dust and uncharged nitriding mix was noted.

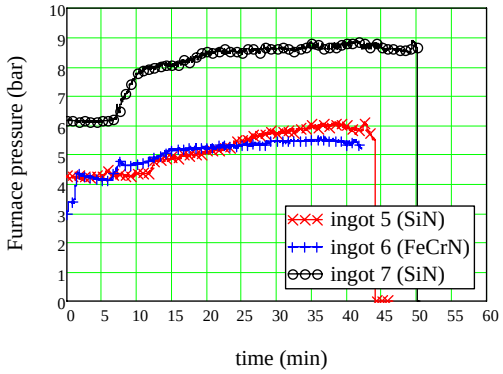

Figure 3: Furnace pressure variation during PESR melts.

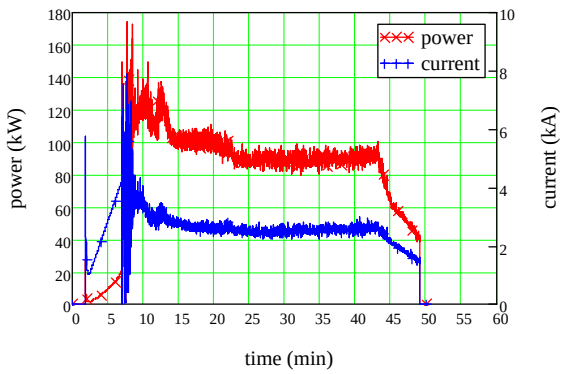

Figure 4: Typical power and current variation the melt (ingot 7).

Results

The three ingots from these trials were sectioned longitudinally and macro-etched. The macro structure from ingot 7 is shown in Figure 5. It is sound and is typical of ESR ingots, with columnar grains from surface to ingot canter at 45 degrees to the vertical axis. The macro structure from the other two ingots was identical to that shown in Figure 5. Next, these plates were cut up into small pieces, 1.25" x 1.25" for x-ray Florence (XRF) analysis followed by optical emission spectrometry (OES) for nitrogen and sulphur analysis. These results for the three ingots are shown in the form of contour plots in Figures 6 thru 8 with the ingot diameter on the horizontal axis, and ingot height on the vertical axis. Note that an ingot height of "0" is the top of ingot. The nitrogen variation shown in Figure 6-a shows that the nitrogen content gradually increases from the bottom of the ingot to a maximum at mid height, and then gradually decreases from mid-height to the very top. The silicon content follows a similar trend as shown

in Figure 6-b. In Figure 7, the results from the ingot with ferro-chrome nitride as additive are shown. The nitrogen content here is considerably higher than that shown in Figure 6-a. It is as high as 1.35 wt%, and exponentially decays to the nitrogen content of the electrode at the very top. The corresponding chromium levels are shown in Figure 7-b, which reaches to as high as 25 wt% at the bottom of the ingot. A quick glance at Figure 7-a also shows a more uniform radial distribution of nitrogen than Figure 6-a. There was no significant change in silicon from ingot 6. Figure 8 shows the measured nitrogen and silicon distribution from ingot 7, where the furnace pressure was highest. Again the nitrogen and silicon were higher at the bottom of the ingot in comparison to the top.

A plot of measured sulphur along the ingot height is shown in Figure 9. The electrode sulphur content was 60 ppm. During the initial stages of the melt, there is effective sulphur removal; however as the ingot grows, the sulphur content gradually increases almost linearly with ingot height.

Figure 5: Macrostructure from ingot 7, higher pressure and Si3N4.

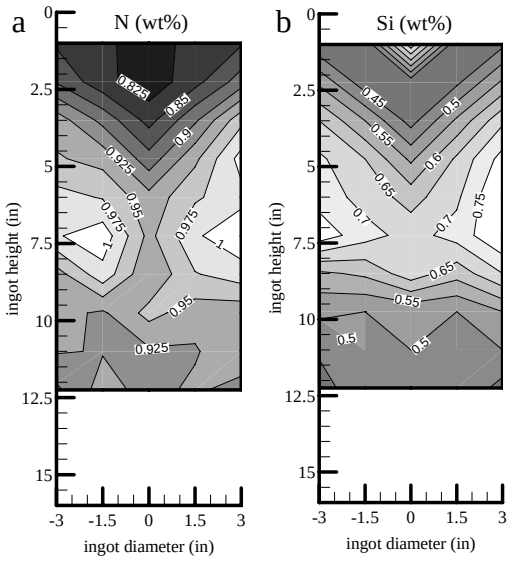

Figure 6: Measured N and Si in ingot 5

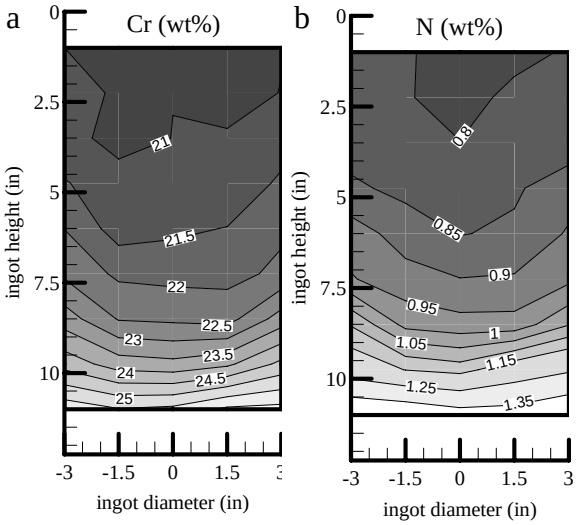

Figure 7: Measured N and Cr in ingot 6

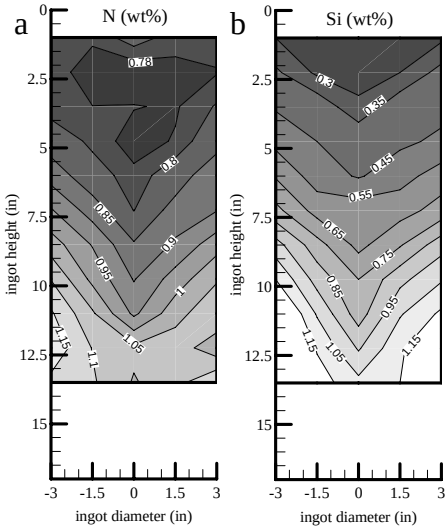

Figure 8: Measured N and Si in ingot 7.

Conclusions

Experiments were on a laboratory scale PESR furnace to examine the effect of furnace pressure and additives on nitrogen solubility in a Fe-Cr-Mn alloy. The results from these initial experiments indicate a gradual decrease in nitrogen as the ingot grows. This is largely attributed to inadequate feeding of the additives during the melt. The melt rate was not uniform during the steady portion of the melt, and the size of additive particles were not optimum for uniform feeding; Si_3N_4 was too fine, and the FeCrN was too coarse.

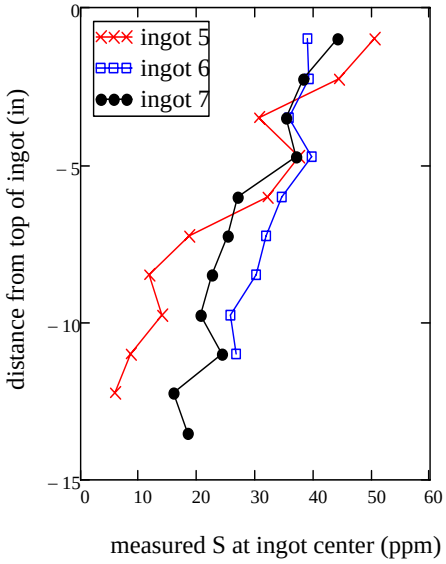

Figure 9: Sulphur variation along the height of the ingot from samples taken from the ingot center.

Another interesting observation from these tests was the nitrogen recovery in these ingots. When FeCrN was used, the ratio of the change in nitrogen to the change in chromium ($\Delta N/\Delta Cr$) was nearly 0.125, which is equal to the ratio of these two elements in the additive. On the contrary, when Si_3N_4, was used, the ratio of the change in nitrogen to the change in silicon ($\Delta N/\Delta Si$) was about 0.3 in both cases at the bottom of the ingot, and this ratio gradually decreases with ingot height. The stoichiometric ratio of nitrogen to silicon in Si_3N_4 is nearly 0.66. This suggests that under these experimental conditions, where both sand and Si_3N_4 were fed together ingot the melt, the nitrogen recovery is lower than using only FeCrN.

The variation in the nitrogen distribution in the radial direction (surface to centre) when Si3N4 was used is attributed to the weak flow in the slag. In larger industrial size units, due to the higher currents, the electromagnetically driven flow in the slag is nearly two to three times stronger than that of the laboratory scale furnaces, and this helps with better mixing of the additive.

Examination of the microstructure using an EDAX detector attached to a Scanning Electron Microscope (SEM) showed sulphide particles, however, no remnant Si_3N_4 or FeCrN was observed.

The degree of desulphurization in PESR can be smaller relative to conventional ESR as sulphur in slag will not be able to react with oxygen in air due to use of nitrogen or inert gas. Sulphur can gradually accumulate in the slag causing a corresponding increase in ingot sulphur level with height. Depending on chemistry requirements, more extensive desulphurization prior to ESR or use of a slag with a higher sulphide capacity may be needed.

References

1. High nitrogen steels," Proc. Of 5th Intl. Conference on High Nitrogen steels", Ed. H. Hanninen, S. Hertzman and J. Romu, Materials Science Forum, Vol. 318-320, 1999.
2. H. K. Feichtinger and G. Stein, "Proc. Of 5th Intl. Conference on High Nitrogen steels", Ed. H. Hanninen, S. Hertzman and J. Romu", Materials Science Forum, Vol. 318-320, 1999, pp 261-270.
3. M. Boh, Proc. Of INTECO symposium, 1999, pp 1-17.
4. A. Mitchell and F. Frederikssom, Proc. Of Intl. Symp. on Liquid Metal Processing and Casting, Ed. P.D. Lee et. al, SF2M, 2003, pp. 109-120.

1 Feichtinger, H.K. and Stein, G., “Melting of High Nitrogen Steels”, *Materials Science Forum*, Vols. 318-320, 1999, pp. 261-270.
2 Lupis, C.H.P., *Chemical Thermodynamics of Materials*, © 1983, Elsevier Science Publishing, Inc., New York, NY.
3 Humbert, J.C. and Elliott, J.F., “The Solubility of Nitrogen in Liquid Fe-Cr-Ni Alloys”, *Transactions of the Metallurgical Society of AIME*, Vol. 218, December 1960, pp. 1076-1088.
4 Pehlke, R.D. and Elliott, J.F., “Solubility of Nitrogen in Liquid Iron Alloys, I. Thermodynamics”, *Transactions of the Metallurgical Society of AIME*, Vol. 218, December 1960, p. 1088.
5 Wada, H. and Pehlke, R.D., “Nitrogen Solution and Titanium Nitride Precipitation in Liquid Fe-Cr-Ni Alloys”, Metallurgical Transactions B, Vol. 8B, September 1977, pp. 443-450.
6 Wada, H. and Pehlke, R.D., “Solubility of Nitrogen in Liquid Fe-Cr-Ni Alloys Containing Manganese and Molybdenum”, Metallurgical Transactions B, Vol. 8B, December 1977, pp. 675-682.
7 Satir-Kolorz, A., “On the Solubility of Nitrogen in Iron and Cast Steel Alloys at Elevated Pressure”, *Giessereiforschung*, 41, no. 4, 1989, pp. 149-165.
8 Anson D.R. et al., “Prediction of the Solubility of Nitrogen in Molten Duplex Stainless Steel”, *ISIJ International*, Vol. 36, No. 7, 1996, pp. 750-758.
9 Shahapurkar, D.S. and Small, W.M., “Nitrogen Solubility in Complex Liquid Fe-Cr-Ni Alloys”, *Metallurgical Transactions B*, vol. 18B, March 1987, pp. 225-230.
10 Rawers et al., “High Nitrogen Concentration in Fe-Cr-Ni Alloys”, *Metallurgical Transactions A*, Vol. 24A, January 1993, pp. 73-82.
11 Rawers, J.C. and Gokcen N.A., “High-Temperature, High-Pressure Nitrogen Concentration in Fe-Cr-Mn-Ni Alloys”, *Steel Research*, Vol. 64, No. 2, pp. 110-113.
12 *Steelmaking Data Sourcebook*, The Japan Society for the Promotion of Science, © 1988, Gordon and Breach Science Publishers, New York.
13 Sigworth, G.K., and Elliott, J.F., “The Thermodynamics of Liquid Dilute Iron Alloys”, *Metal Science*, Vol. 8, 1974, pp. 298-310.